



Influence of Nanoscale Marble (Calcium Carbonate CaCO_3) on Properties of D600R Surfacing Electrode

Nanoscale marble was added to the flux coating of D600R, a newly developed hardfacing electrode for the repair of steel rolls

BY B. CHEN, F. HAN, Y. HUANG, K. LU, Y. LIU, AND L. LI

ABSTRACT

Conventional microscale marble in the flux coating of D600R, a hardfacing shielded metal-arc welding electrode, was replaced by marble of nanoscale sizes for possible enhanced electrode characteristics. The microscale marble was substituted with different proportions of nanoscale marble particles. An arc characteristics analyzer was used to measure the welding current, arc voltage, and short-circuiting characteristics of the electrode under various welding conditions. Hardness and wear resistance properties of the weld deposit were characterized. The results show that the smaller marble particle sizes in the flux coating produced lower short-circuiting voltage, lower short-circuiting current, and shorter short-circuiting time. A significantly improved arc stability resulted in better welding characteristics of the electrode. The nanoscale marble particles in flux coating produced greater metal deposition efficiency, as well as increased hardness and wear resistance of the deposit.

B. CHEN and F. HAN are with Wuhan University of Technology, Department of Material Process Engineering, Wuhan, China. Y. HUANG is with Sinosteel Xingtai Machinery & Mill Roll Co., Xingtai, Hebei, China. K. LU and Y. LIU are with Wuhan Anchor Welding Consumables Co., Wuhan, China. L. LI is with Department of Mechanical & Aerospace Engineering, Utah State University, Logan, Utah (leijun.li@usu.edu).

Introduction

Due to their small size and large surface effects, nanomaterials have unique mechanical, electrical, magnetic, and optical properties differing from traditional materials (Refs. 1–8). These properties enabled nanomaterials to be used in an array of applications, including the defense, electronic, aerospace, and chemical industries. The introduction of nanotechnology to welding started at the end of the 20th century. There are currently commercial welding consumables that contain nanomaterials. Although systematic studies on the roles of nanomaterials during welding process are still missing, a few research papers are available on nanomaterial-containing welding consumables (Refs. 9–12).

In this investigation, nanoscale marble particles were added to the flux cover of D600R hardfacing welding electrodes, partially or entirely substituting the original (microscale) marble particles. The hypothesis was the small size of the nanoscaled marble particles, with an effective constituent of CaCO_3 , will significantly affect the chemical reactions in the slag, and change the properties of the flux coating. An investigation was conducted on the effect of concentration of nanoscale marble in flux coating on the welding procedural and metallurgical properties of a hardfacing electrode. The melting charac-

ter, which includes the melting temperature and its range, was investigated for the experiment electrodes. The effects of nanoscale marble on the length of flux sleeve, stability of electric arc, formation of weld bead, and adaptability for all-position welding were characterized.

Experimental Procedure

The D600R is a newly developed electrode for the repair of steel rolls. The core of the electrode is H08A steel, with a nominal composition of C < 0.1%, Mn 0.3–0.55%, Si < 0.03%, Cr < 0.2%, Ni < 0.3%, S and P < 0.03%. The composition of the flux system for D600R is kept constant, except the conventional, microscaled marble was replaced with nanoscaled particles. The composition of the flux is listed in Table 1, and replacement ratios for nanoscale marble are given in Table 2.

A Model TL-25 hydraulic electrode extrusion machine was used to produce the experimental electrodes. No apparent effect was observed of nanoscale marble on the extrusion behavior of the electrodes. The flux coating has sufficient strength, moisture resistance, and smooth appearance. The electrodes were dried according to the following sequence: at room temperature for 24 h, at 50°C for 7 h, at 120°C for 3 h, at 250°C for 2 h, and finally at 380°C for 1.5 h.

A high-temperature physical properties measurement device (Model GX) was used to measure the melting range of the fluxes. The mixed fluxes were made into cylinders 3 mm in diameter and 3 mm high. The specimen was sealed in the test chamber that was filled with Ar. The contour of the specimen and temperature indication were recorded digitally as shown in Fig. 1. The heating current was 4–5 A,

KEYWORDS

Welding Electrode
Flux Coating
Nanoscaled Marble
Calcium Carbonate



Fig. 1 — The contour of the specimen and temperature indication before heating test.

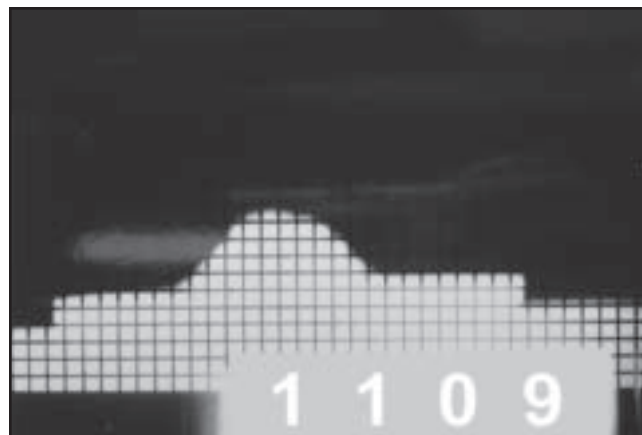


Fig. 2 — The specimen with its height collapsed to half of the original height at the melting temperature.

Table 1 — Composition of Flux Coating of Electrode D600R

Flux Constituent	Percentage (wt-%)
Marble	31
Fluorite	36
High carbon ferromanganese	3
Carbon ferrochromium	14
Ferromolybdenum	2
Rare-earth silicoferrite	1.5
Ferrotitanium	10
Sodium carbonate	1.5
Graphite	0.5
Light rare-earth oxide	1

Note: The total amount by weight of the flux constituents is 100.5%; water glass: sodium silicate with density 1.49–1.51 g/cm³ and modulus M = 2.9–3.0; electrode core wire is steel H08A with 4.0-mm diameter; extrusion die throat-diameter is 6.8–6.9 mm.

Table 2 — Concentration of Nanoscale Marble and Electrode Properties

Flux ID	Nanoscale Marble (%)	T _m (°C)	Melting Range (°C)	Sleeve Length (mm)
HT1	0	1110	80	1.73
HT2	10	1098	40	1.62
HT3	20	1073	24	1.10
HT4	25	1063	26	1.08
HT5	50	1082	38	1.15
HT6	100	1079	76	1.13

and the heating rate was 10–15°C/min. The change of contour in the specimen during heating and melting was observed and recorded. The effective melting point of the fluxes was defined as the temperature at which the fluxes start to melt. This effective melting temperature was measured when the specimen height collapsed to one-half of the original height upon heating — Fig. 2. The melting temperature range was defined as the temperature between the start of the specimen collapse and the melting point defined above.

The deposit (cladding) efficiency tests were conducted on the low-carbon steel plates (dimensions 400 × 50 × 10 mm). Three electrodes were used for each test on three plates, and the remaining length

the electrode was about 50 mm. The length of electrode and weight of plate were measured before welding. The remaining length of the electrode, weight of the electrode core, and weight of the test plate were also measured after welding. The error of measurement was below 0.1 g. The equation for the deposit efficiency calculation was (Ref. 14)

$$\text{Deposit efficiency} = \frac{\text{deposit metal weight (g)}}{\text{total weight of 3 melted electrode cores (g)}} \times 100\%$$

where deposit metal weight (g) = plate weight after welding (g) – plate weight before welding (g).

The diffusible hydrogen content in the weld bead was measured according to standard GB-T3965—1995, *Measurement Methods for Diffusible Hydrogen in the Electrode Deposit Metal*, which is similar to ISO 3690. The diffusible hydrogen results obtained using GB-T3965 are comparable to those obtained from ISO 3690. The distribution of arc voltage probability density is generated by the Hanoverian electric arc quality analysis device (Ref. 17). The bead-on-plate welding was conducted on the Q235 low-carbon steel plate (400 × 50 × 10 mm). Each test was repeated three times. The sampling time used was 5 s. The density distribution of the probability $n\%$ of arc voltage occurring randomly was recorded for the given time.

Results and Discussion

Melting Characteristics

The effective melting point (T_m) and melting temperature range of the test flux coatings are shown in Table 2. The addition of nanoscale marble had the effect of decreasing the melting point and melting temperature range of the flux coating. As the concentration of nanoscale marble increased, the melting point and melting temperature range increased. HT4 had the lowest melting point (1063°C). The melting ranges of HT3 and HT4 are narrow, being 24°C and 26°C, respectively. HT1 and HT6 have wider ranges of melting temperature, being 80°C and 76°C, respectively. A decreased melting point makes the formation of a long flux sleeve on the end of an electrode difficult. It was found that the variations of the flux sleeve length and melting point have the same trend, i.e., the Flux HT4 (with 25% nanoscale marble) has the shortest flux sleeve. Maintaining similar welding conditions, electrodes with shorter sleeve length tend to produce less penetration. For a hardfacing electrode, minimization of di-

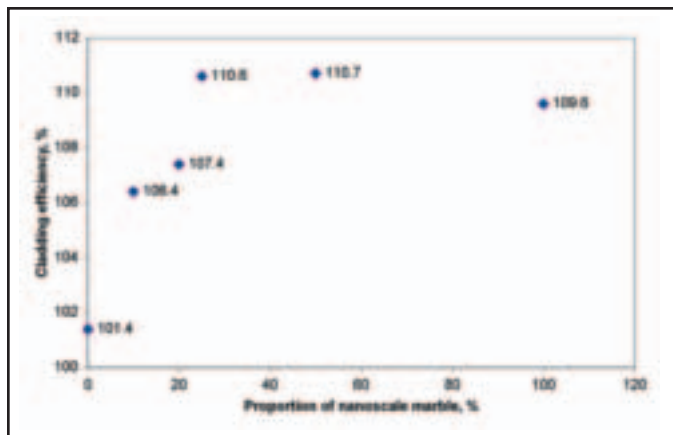


Fig. 3 — Deposit (cladding) efficiency of electrodes vs. proportion of nanoscale marble in flux.

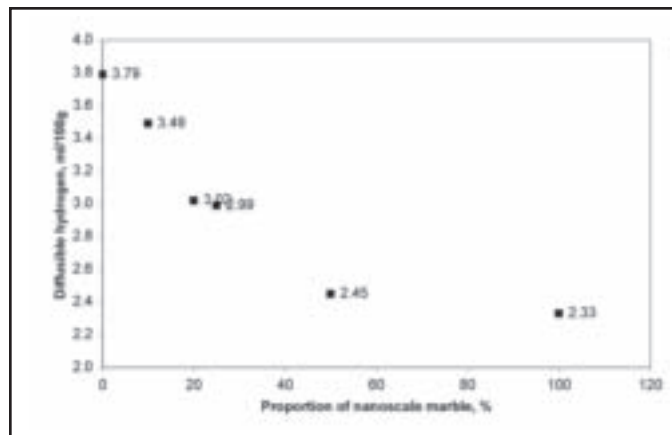


Fig. 4 — Diffusible hydrogen content in the deposit metal vs. proportion of nanoscale marble.

Table 3 — Chemical Composition of Fusion Deposit of Electrodes (wt-%, Balance Is Fe)

Flux ID	C	Mn	Si	P	S	Cr	Mo
HT1	0.49	0.95	0.34	0.017	0.005	3.58	0.50
HT2	0.55	1.09	0.22	0.017	0.005	3.74	0.53
HT3	0.57	1.12	0.32	0.017	0.005	3.85	0.56
HT4	0.56	1.06	0.32	0.016	0.005	3.71	0.50
HT5	0.52	0.97	0.33	0.017	0.005	3.42	0.48
HT6	0.53	1.00	0.34	0.017	0.005	3.54	0.49

lution due to deep penetration may be desired. Nanoscale marble provides an additional method to control the penetration through the sleeve length design.

The changes in melting temperature and its range are believed to be caused by two effects. First, nanoscale marble with more surfaces will decompose more completely into CaO, which may increase the melting point of the electrode flux. Second, the increased surface areas may also cause nanoscale particles to absorb arc energy more efficiently. Thus, adding nanoscale marble may decrease the melting point of the flux. For different proportions of nanoscale marble, one of the effects may dominate. This would account for the changes in melting point and melting temperature range.

Deposit Efficiency

The deposit efficiency varying with the nanoscale marble is shown in Fig. 3. The deposit efficiency increases with the increasing portion of nanoscale marble. When the portion of nanoscale marble is more than 25%, the deposit efficiency reaches a plateau with a small decrease, until the marble is entirely substituted with nanoscale marble. HT4 and HT5 have the higher deposit efficiencies, which are 110.6% and 110.7%.

When the alloy components are transferred from the coating to the weld bead, the equilibrium is (Ref. 15)

$$M_d = M_o - (M_{sl} - M_{ox})$$

where M_d is the amount of alloy transferred to deposit; M_o is the initial amount of the alloy in the electrode (core and flux coating); M_{sl} is the remaining amount of the alloy in the slag; and M_{ox} is the amount of the oxidized alloy. With more instant generation of CO_2 caused by more nanoscale marble added, the stirring effect of the weld pool may be increased, and the remaining amount of alloy components in slag M_{sl} decreases. Meanwhile, the increasing oxidation effect increases the amount of alloys that are lost by oxidation. These two potentially competing effects would determine the final amount of alloy components transferred to the weld pool. The chemical composition of the fusion deposit of the test electrodes indicates such an effect (Table 3). The concentration of alloying elements first increases then decreases with an increasing portion of nanoscale marble in the fluxes.

Diffusible Hydrogen Content

The content of diffusible hydrogen in the deposit metal decreases with the increase of nanoscale marble in the flux — Fig. 4. When nanoscale marble is more than 50%, the diffusible hydrogen level reaches a low plateau. The reason for the beneficial effect of nanoscale marble is believed to be related to the increased surface areas of the particles. More CO_2 is

Table 4 — Arc Stability Measured Using Analytator Hanover

Flux ID	ΣU_s (%)	ΣI_s (%)	ΣT_1 (ms)
HT1	7.56	35.80	176
HT2	7.48	32.05	175
HT3	7.12	30.55	170
HT4	6.57	28.83	156
HT5	6.57	29.72	159
HT6	6.94	29.39	156

generated by the decomposition of fine marble ($CaCO_3$), and the effect of oxidation is enhanced. The partial pressure of hydrogen is reduced due to an increased CO_2 partial pressure. A strong relation exists between the partial pressure of hydrogen and the solubility of hydrogen in the deposit metal (Refs. 15, 16).

Arc Stability and Metal Transfer

The distributions of arc voltage probability density for the test electrodes under the same welding parameters are shown in Fig. 5. The probability density (n , %) is a function that represents a probability distribution in terms of an integral. The probability for arc voltage to fall between, for example, 4 and 6 volts, equals the area underneath the curve (i.e., integration) between the 4 to 6 interval. All the distributions of arc voltage probability density have a similar shape of two peaks. The left peak describes the probability density distribution of the short-circuit voltage for coarse drop short-circuit transfer (Refs. 17–19). Therefore, the smaller the left-peak area, the better the arc stability for the electrode.

The area of the left peak was integrated from the minimum voltage to the minimum probability value between two peaks. This integrated probability is defined as ΣU_s (%). It can be used as a parameter for evaluating the short-circuit droplet transfer. A smaller ΣU_s means

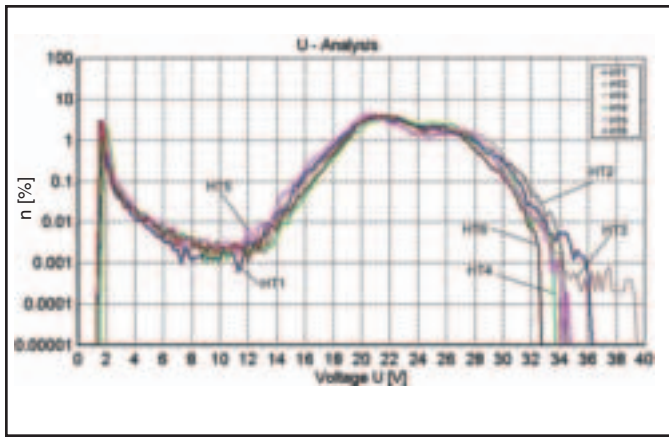


Fig. 5 — Voltage probability density.

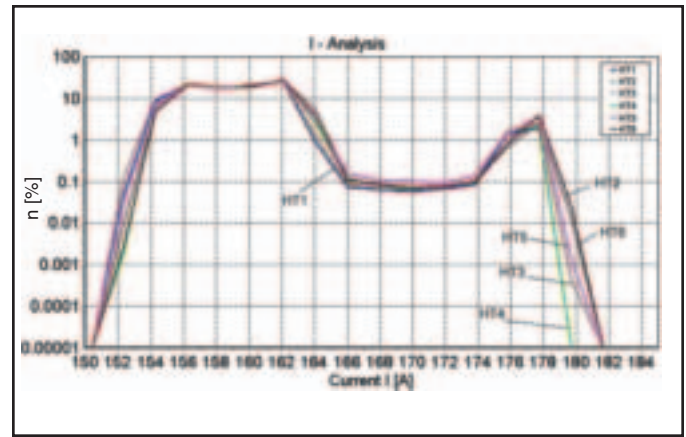


Fig. 6 — Comparison of current probability distributions of test electrodes.

Table 5 — Hardness and Abrasive Wear Resistance of Test Electrodes

Flux ID	Deposit Metal Hardness, (HRC)	Abrasion Weight Loss (g)
HT1	58.3	0.021
HT2	59.6	0.018
HT3	60.4	0.008
HT4	62.1	0.005
HT5	61.2	0.011
HT6	60.1	0.016

less of a chance for short-circuit and explosion drop transfers. Table 4 shows the ΣU_s for the test electrodes. HT4 has the smallest ΣU_s , which is 6.57%. HT4 has a more stable arc, with less splash, and better processing properties. While the ΣU_s for HT1 is the largest (7.56%), creating a greater tendency for short-circuit and explosion drop transfer.

The distributions of welding current probability density for the test electrodes are shown in Fig. 6. The rising part on the left portion of the curves shows the distribution of welding current probability density for the moment of the end of short circuit and the re-ignition of the arc. The next portion of the curves shows the distribution of welding current probability density for the period of the stabilized arc, which has the maximum probability density. The rest of the curves represents the period of short-circuiting. It has the maximum current when the molten drop contacts the weld pool. The higher the curve intersects with the current axis (horizontal), the higher the short-circuit current (Refs. 20, 21). All the distribution curves for the electrodes share a similar shape and the probability density decreases after 162 A. The short-circuit current probability densities (ΣI_s) above 162 A for test electrodes have been calculated and shown in Table 4. The sum of short-circuit current probability density ΣI_s for HT4 is 28.83%, much smaller compared with others. It shows that less short-circuit transfer

and explosion transfer exists for HT4 and it has better arc stability. Flux HT1 has the maximum ΣI_s (35.80%), so it has worse arc stability. The reason for HT4 to have shown a lower short-circuit current than other fluxes, especially HT3, is not clear. One reason may be that the small variations in the arc length during testing have affected the arc voltage and current.

The short-circuit time T_1 is the time from the contact of the liquid drop with the weld pool to the detachment. The larger molten drop has the longer short-circuit time. Thus, the short-circuit time reflects the size of the liquid drop. Among the frequency distributions of short-circuit time T_1 , a threshold of 2.05 ms has been used to separate the short-circuit probability distribution (Ref. 18). The short-circuit time $T_1 \leq 2.05$ ms corresponds to fine droplet transfer in the slag bridge, while the short-circuit time $T_1 > 2.05$ ms corresponds to coarse droplet short-circuit transfer. The total short-circuit time T_1 , defined as the accumulated short-circuit time for $T_1 > 2.05$ ms, can be used as an arc stability parameter. The shorter the T_1 , the more stable the welding arc. The T_1 data for all electrodes are calculated and listed in Table 4. The largest ΣT_1 is for HT1 with 175.9 ms, while all the ΣT_1 time for the electrodes with nanoscale marble added are shorter than HT1. Flux HT4 has the shortest ΣT_1 , which is 155.5 ms. Thus, the nanoscale marble can shorten the short-circuiting time.

Deposit Metal Properties

The microstructure was observed using an Olympus™ BX51M microscope. Specimens were prepared according to standard metallographic preparation method. It was found that there was no significant difference in the microstructure of the deposit metal. The structure is needle martensite, retained austenite, and some carbide — Fig. 7.

In Table 5, the average hardness numbers and wear resistance results are listed. Flux HT4 has the highest hardness, while HT1 has the lowest. The averaged hardness of the deposit metal with nanoscale marble added is slightly higher than that with microscale marble. The distribution of hardness is more uniform throughout the deposit metal with nanoscale marble added. The difference between the maximum and minimum hardness values is 7 HRC for HT1, while the difference is only 3 HRC for HT6.

The abrasive resistance tests were conducted on a Model MM-200 continuous sliding dry abrasion machine. The deposit metal from test electrodes was machined into 1-mm-diameter, 15-mm-high pin specimens. The pin specimen slid against the outer surface of a 40-mm-diameter cylinder made from a 0.45% C steel, machined and quenched to a hardness of HRC 60. During the test, the pin specimen was held stationary with its rotational axis perpendicular to that of the 40-mm steel cylinder, which rotated at 200 rev/min, and a load of 98 N was applied to the pin specimen. The abrasive wear test did not involve a lubricant. The test procedure was the following: The pin specimen was first wear tested for 15 min; then it was removed from the machine, cleaned, dried, and weighed for the initial weight. The specimen was then tested for 120 min. The tested specimen was cleaned, dried, and weighed for the postwear weight. The abrasive resistance was evaluated by

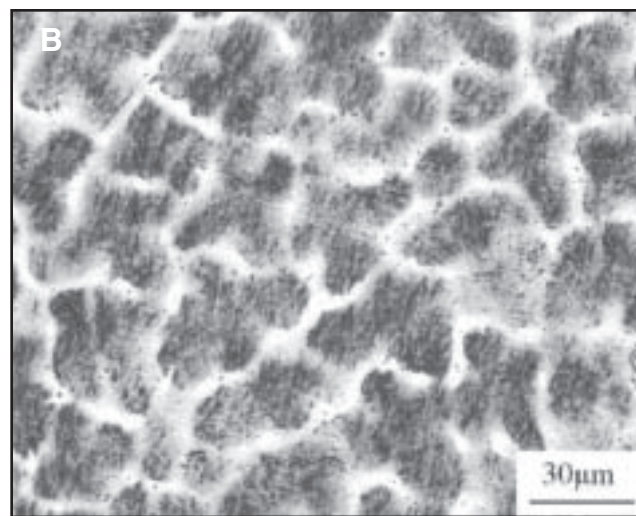
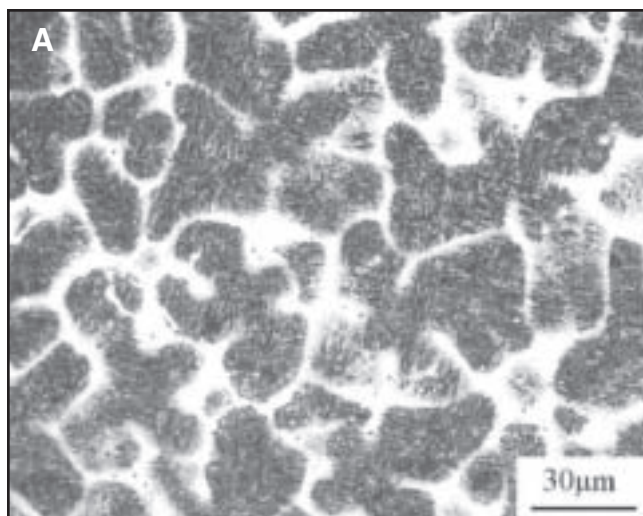


Fig. 7 — The as-deposited microstructure. A — Electrode with HT1 coating (microscale marble); B — electrode with HT6 coating (100% nanoscale marble). 4% Nitral etch.

weight loss. The weights of the sample before and after the abrasion test were measured on an analytical scale, with a precision of 0.0001 g. Each measurement was repeated at least three times, and the average value was reported. The variation between the readings in weight was ± 0.0002 g. Shown in Table 5, the increase of nanoscale marble in the coating improves the abrasive resistance of the deposit sample. Specimen HT4 has the best abrasive resistance and HT1 with zero nanoscale marble has the worst wear resistance.

Conclusions

The introduction of nanoscale marble (calcium carbonate) has a significant influence on the properties of D600R shielded metal arc welding electrode flux. The stability of the electrical arc, content of diffusible hydrogen in the deposit metal, and deposit efficiency are improved by replacing the conventional (microscale) marble with nanoscale marble in the electrode flux coating. The nanoscale marble improves the hardness and abrasive resistance of the deposit metal. The optimum proportion of the nanoscale marble seems to be between 20 and 25% for both the arc stability and deposit metal properties.

Acknowledgment

This paper is based on a conference article and reprinted with permission of *Materials Science & Technology 2008 Conference & Exhibition Proceedings*.

References

1. Yang, Z. Y. 2004. *Nanotechnology*, Beijing, Mechanical Engineering Press.
2. Zhang, Q. Q., and Zhang, J. W. 2005. *New Development in Nanotechnology*, Beijing, Defense Industry Press.
3. Aizawa, T., and Kondoh, K. 2001. Nanostructured materials via bulk mechanical alloying. *Scripta Mater.*, 44: 1751–1755.
4. Aizawa, T. 2000. Nanogranulation process into magneto-resistant Co–Cu alloy on the route of bulk mechanical alloying. *Materials Science and Engineering*, A285, 1–7.
5. Xu, G. C., and Zhang, L. D. 2002. *Nanoscale Complex Material*. Chemical Industry Press, Beijing.
6. Kear, B. H., and Strutt, P. R. 1995. Chemical processing and application of nanostructured materials. *Nanostructured Materials*, 6(1): 227–236.
7. Rawers, J. C. 1998. Thermal stability of nano-structured metal alloys. *Thermal Spray Tech.*, 7(3): 427–428.
8. Tao, N. R., Sui, M. L., and Lu, K. 1999. Surface nano-crystallization of iron induced by ultrasonic shot peening. *Nano-structured Materials*, 11(4): 433–440.
9. Yang, D. X., Zhao, X. J., and Chen, C. H. 2003. Investigation of application of nanoscaled W-FeC powder in fusion welding. *Mechanical Engineering Materials*, 27(2): 36.
10. Zhao, X. J., Yang, D. X., and Chen, C. H. 2003. D707 electrode with nanoscaled compound powder. *Hard Alloys*, 20(2): 76–79.
11. Chen, C. H., Zhao, X. J., and Shi, C. Y. 2003. Using nanoscaled powder for developing new hardfacing welding electrode. *Transactions of Dalian Railway Institute*, 24(1): 52–56.
12. Zhao, X. J. 2003. Chromium carbide nanoscaled powder used in a hardfacing weld electrode. *Thermal Processing Techniques*, (3): 27–28.
13. Zhang, Q. H., Wu, X. P., and Hong, B. 2002. *Welding Filler Materials Development Theory and Techniques*. Beijing, Metallurgical Industry Press.
14. Zhang, Z. R., and Li, S. H. 1998. *Welding Electrodes*. Beijing, Mechanical Engineering Press.
15. Zhang, W. Y. 1999. *Welding Metallurgy (Fundamental Principles)*. Beijing, Mechanical Engineering Press.
16. Tang, B. G., Ying, S. K., and Wang, Y. R. 1987. *Welding Filler Materials for Low-Carbon and Low-Alloy High-Strength Steels*. Beijing, Mechanical Engineering Press.
17. Song, L., and Wang, B. 2006. Shielded flux-cored wire welding under various welding parameters. *Transactions of Zhongbei University*, 27(1): 83–85.
18. Gao, J. H., Wang, B., and Song, L. 2006. Analysis of arc physics of a fluoride-type carbon steel welding electrode. *Welding*, (10): 51–54.
19. Rehfeldt, D. D., and Rehfeldt, M. D. 2003. Computer-Aided Quality Assurance (CAQ) of Al-MIG-welding with Analysator Hanover. *Proc. International Forum on Automobile Welding*, Beijing, Mechanical Engineering Press.
20. Yang, L., and Wang, B. 2004. Analysis of several flux-cored welding wires using the Hanover Welding Quality Analyzer. *Welding Equipment and Materials*, 33(5): 38–42.
21. Wang, B., Yang, L., and Wang, Y. 2006. Critical analysis of droplet transfer modes for welding electrode. *Transactions of Welding*, 27(11): 95–98.

Change of Address? Moving?

Make sure delivery of your *Welding Journal* is not interrupted. Contact the Membership Department with your new address information — (800) 443-9353, ext. 217; smateo@aws.org.